Acta Crystallographica Section B
Structural Science
ISSN 0108-7681

A new structure type in the hexagonal perovskite family; structure determination of the modulated misfit compound $Sr_{9/8}TiS_3$

O. Gourdon,[a] V. Petricek[b] and M. Evain[a]*

[a]Laboratoire de Chimie des Solides, IMN, UMR C6502 CNRS, Université de Nantes, 2 rue de la Houssinière, BP 32229, 44322 Nantes CEDEX 3, France, and [b]Institute of Physics, Academy of Sciences of the Czech Republic, Na Slovance 2, 182 21 Praha 8, Czech Republic

Correspondence e-mail: evain@cnrs-imn.fr

Received 29 November 1999
Accepted 7 February 2000

$Sr_{9/8}TiS_3$, strontium titanium sulfide, a new phase in the hexagonal perovskite-like Sr_xTiS_3 system, has been prepared and its structure solved from single-crystal X-ray data within the (3 + 1)-dimensional [(3 + 1)D] formalism. $Sr_{9/8}TiS_3$ crystallizes with trigonal symmetry [$R\bar{3}m(00\gamma)0s$ superspace group], with the following lattice parameters: a_s = 11.482 (3), c_s = 2.9843 (8) Å, $\mathbf{q}$ = 0.56247 (7)$\mathbf{c}^*$ and V_s = 340.7 (3) Å^3. The structure was considered as commensurate [$R\bar{3}c$ three-dimensional (3D) space group], but refined within the (3 + 1)D formalism to a residual factor R = 2.79% for 64 parameters and 1084 independent reflections. Original crenel functions were used for the sulfur and strontium description. The structure is different from that of the hexagonal perovskite-like oxide counterparts. The main difference is related to the presence of a new type of polyhedron in the [MS_3] transition metal chains, intermediate between the octahedra classically found in such chains and the trigonal prismatic sites encountered in the oxides.

1. Introduction

In the hexagonal perovskite family of the general formula A_xMO_3 (A = Sr, Ba *etc.* and M = Co, Ni *etc.*), numerous compounds have been synthesized and characterized (see for instance Perez-Mato *et al.*, 1999, and references therein). Their crystal structures can be described either as a stacking of mixed [A_3O_9] and [$A_3M^{II}O_6$] layers with M^{IV} elements occupying the octahedral sites between these layers, the M^{II} cations filling trigonal prismatic sites (Darriet & Subramanian, 1995; Dussarat *et al.*, 1995), or as intergrowth compounds with two chain subsystems: an [MO_3] first chain subsystem with a varying succession of face-sharing [$M^{IV}O_6$] octahedra and [$M^{II}O_6$] trigonal prisms, and an [A] second chain subsystem (Ukei *et al.*, 1993; Onoda *et al.*, 1993). Recently, precise structure determinations using advanced crystallographic models have shown the unity of the series and evidenced some peculiar characteristics, such as the instability of Ni^{II} and Co^{II} in their trigonal prismatic sites, with a displacement of the cations out of the site centre. To our knowledge, the analogous sulfide compounds are much more limited and their structures poorly characterized. Saeki and co-workers have reported the existence of a composition range for the Sr_xTiS_3 (x = 1.05–1.22; Saeki *et al.*, 1993), Ba_xTiS_3 (x = 1.00–1.05; Saeki & Onoda, 1994) and $BaTiS_y$ (y = 2.70–2.93; Saeki *et al.*, 1996) compounds, and one crystal structure, $Sr_{1.145}TiS_3$ (Onoda *et al.*, 1993), has been determined from powder diffraction data. However, such a structure should be considered cautiously. Indeed, structure refinements from powder diffraction data might not be the most accurate method to choose when several very close

compositions can be obtained simultaneously (for instance, in the Sr–Co–O system, $Sr_{14/11}CoO_3$ and $Sr_{24/19}CoO_3$ single crystals have been found in the same homogeneous-looking batch), leading to possible line broadening and structure averaging. In fact, the Sr_xTiS_3 structure is reported to be similar to that of the hexagonal perovskite-like oxides, with a succession of octahedra and trigonal prisms in the $[TiS_3]$ chains. This is surprising and questionable, given the usual coordination of titanium in a sulfur environment. The presence of Ti^{II} in the trigonal prisms, if one assumes the same charge balance as in the oxides, is even more questionable.

To elucidate the crystal structures of the hexagonal perovskite sulfides, research was initiated on the Sr_xTiS_3 and Eu_xTiS_3 systems. The quest for large enough single crystals led to the characterization of three new phases, namely $Sr_{9/8}TiS_3$, $Sr_{1.1054}TiS_3$ and $Eu_{8/7}TiS_3$, besides the already reported $Sr_{8/7}TiS_3$ phase; single crystals suitable for conventional X-ray diffraction techniques were obtained for each phase. Since the structure analyses of $Sr_{8/7}TiS_3$ and $Eu_{8/7}TiS_3$ are hampered by a particular twinning and the description of the $Sr_{1.1054}TiS_3$ structure is specific because of its very long period, we report herein the structure determination of $Sr_{9/8}TiS_3$, a new modulated phase in the Sr_xTiS_3 family. In addition, we compare the refined structure model to that found for the oxide analogues and emphasize the peculiar atomic arrangement found for $Sr_{9/8}TiS_3$, probably common to all phases in the hexagonal perovskite-type titanium sulfides.

2. Experimental

2.1. Synthesis and characterization

$Sr_{9/8}TiS_3$ single crystals were obtained from a mixture of the elements [Sr:Ti:S = 1.2:1:3; Sr metal ($\leq$ 6 mm pieces), 99.95% (Cerac); Ti sponge powders, 99.9% (Cerac); S powder, >99.999% (Flucka)]. The mixture was placed in a sealed evacuated silica tube at 723 K for 2 d. The furnace was subsequently brought to 1273 K, and kept at that temperature for 4 d. After natural cooling of the closed furnace, the products were ground for homogenization and reheated for crystallization, again at 1273 K for 4 d. Small crystalline unshaped blocks with a metallic luster were then obtained. Energy dispersive X-ray spectrometry (EDXS) analyses of the polished surfaces by means of a Jeol microscope (TRACOR-TN 5500 equipped Jeol-JSM35C) gave a formula close to $Sr_{1.15}TiS_3$, confirming the homogeneity of the phase and the absence of impurities.

2.2. Data collection

Given the desired quality of the structure determination, special care was devoted to the search for a good diffracting single crystal. Because of the lack of well shaped crystals with easily identified faces, the blocks had to be cut to proper dimensions. A first crystal selection was achieved by using a Weissenberg camera. Then the crystals giving the best quality diffraction spots were further analysed with a Stoe image-plate system (IPDS). The best crystal was selected and subsequently used for two different data collections. Firstly, the weaker intensities (main reflections and satellites) at low $\sin(\theta)/\lambda$ (up to 0.57 Å^{-1}) were collected on the IPDS with long exposure periods. Then the stronger intensities (main reflections of the two subsystems only) in a larger $\sin(\theta)/\lambda$ range (up to 0.8 Å^{-1}) were measured on a traditional Nonius CAD-4*F* diffractometer. Both sets, obtained with the same crystal orientation, were in agreement with trigonal symmetry and a metric that could be described in a 3D hexagonal Bravais *R*-centred lattice ($a \simeq 11.48$ and $c \simeq 47.7$ Å). The misfit character of the structure was obvious from the diffraction patterns, with two subsystems of main reflections and satellites. From 622 reflections obtained with the IPDS and a (3 + 1)D indexing, the least-squares refinement of the system metric with the program *U-FIT* (Evain, 1992) gave the following lattice parameters: $a_s = 11.482$ (3), $c_s = 2.9843$ (8) Å, $\mathbf{q} = 0.56247$ (7)$\mathbf{c}^*$ and $V_s = 340.7$ (3) Å^3. The reflection indices of the $[TiS_3]$ first subsystem and the [Sr] second subsystem are obtained from the (3 + 1)D superspace indexing *via* the following $\mathbf{W}^1$ and $\mathbf{W}^2$ transformation matrices, respectively:

$$\mathbf{W}^1 = \begin{pmatrix} 1 & 0 & 0 & 0 \\ 0 & 1 & 0 & 0 \\ 0 & 0 & 1 & 0 \\ 0 & 0 & 0 & 1 \end{pmatrix} \quad \text{and} \quad \mathbf{W}^2 = \begin{pmatrix} 1 & 0 & 0 & 0 \\ 0 & 1 & 0 & 0 \\ 0 & 0 & 0 & 1 \\ 0 & 0 & 1 & 0 \end{pmatrix}.$$

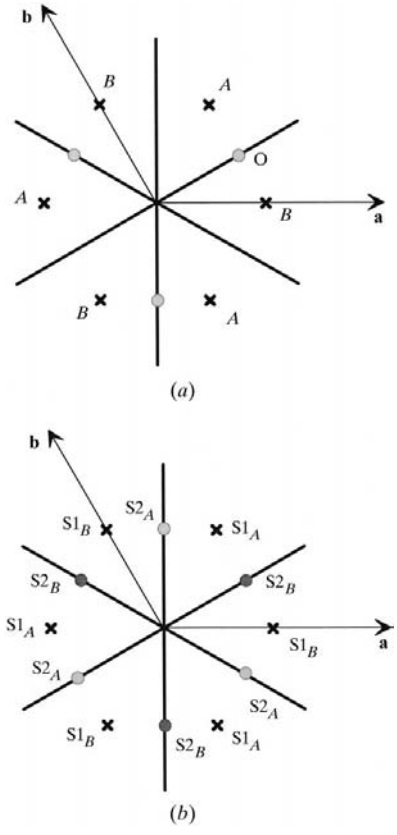

Figure 1
Projection along *c* onto the *ab* plane of (*a*) the oxygen displacements (*A* and *B*) away from the basic position (O) in $Sr_{1.2872}NiO_3$ (Evain *et al.*, 1998) and comparatively (*b*) the sulfur split positions in $Sr_{9/8}TiS_3$ (see text for details).

Table 1
Crystallographic data for $Sr_{1.125}TiS_3$.

(*a*) Physical, crystal and analytical data

	(3 + 1)D option	[3D option]
Formula	$Sr_{1.125}TiS_3$	$[Sr_9Ti_8S_{24}]$
M_r	242.63	[1941.04]
Crystal system	Trigonal	
Space group (*t* section)	$R\bar{3}m(00\gamma)0s$	$R\bar{3}c$ (t = 0)
a (Å)	11.482 (3)	
c (Å)	2.9843 (8)	[47.749 (13)]
	$\mathbf{q} = 0.5625\mathbf{c}^* \simeq (9/16)\mathbf{c}^*$	
V (Å^3)	340.7 (3)	[5451 (5)]
Z	3	6
D_x (g cm^{-3})	3.553	
Cell parameter determination	From 642 reflections, 2θ positions obtained from the IPDS measurement	
Crystal description	Black metallic block	
Crystal size (mm)	~0.012 × 0.08 × 0.08	
Temperature (K)	293	

(*b*) Data collection

	Enraf–Nonius CAD-4*F*	Stoe IPDS
Monochromator	Oriented graphite (002)	Oriented graphite (002)
Radiation	Mo K–$L_{2,3}$ (λ = 0.71073 Å)	Mo K–$L_{2,3}$ (λ = 0.71073 Å)
Scan mode	$\omega/2\theta$	ω
No. of measured reflections	3687	24 448
hkl range	$-18 < h < 18$	$-14 < h < 15$
	$-18 < k < 18$	$-15 < k < 15$
	$-64 < l < 64$	$-62 < l < 62$
$\sin(\theta)/\lambda$ range (Å^{-1})	0–0.8	0–0.57
No. of standard reflections	3	Not applicable
Frequency of standard reflections (s)	3600	Not applicable

(*c*) Data reduction

	Enraf–Nonius CAD-4*F*/Stoe IPDS
Linear absorption coeffcient (cm^{-1})	161.4
Absorption correction	Analytical
T_{min}/T_{max}	0.11/0.17†
No. of reflections	28 135
No. of independent reflections	1643
Criterions for observed reflections	$I > 2\sigma(I)$
No. of observed reflections	1084
R_{int} (observed reflections)	0.0579

(*d*) Refinement

	Commensurate (3 + 1)D option	[3D option]
Refinement coefficient	F^2	
F(000)	338	[5412]
No. of reflections used in the refinement	1084	
No. of refined parameters	64	
R (%) = $\sum\|\|F_{obs}\| - \|F_{calc}\|\|/\sum\|F_{obs}\|$	2.79	
wR (%) = $[\sum w(\|F_{obs}\|^2 - \|F_{calc}\|^2)^2/\sum w\|F_{obs}\|^4]^{1/2}$	4.94	
S	0.84	
Weighting scheme	$w = 1/[\sigma^2\|F_{obs}\| + (0.016\|F_{0obs}\|)^2]$	
$\Delta\rho_{min}$, $\Delta\rho_{max}$ (e Å^{-3})	−1.6, +1.7	

† 0.10/0.17 for Stoe IPDS, all other values are combined.

For a comprehensive description of $(3+n)$-dimensional crystallography, see, for instance, works by Janssen *et al.* (1993) and van Smaalen (1995), the latter being more specific for intergrowth compounds. As the γ component of the **q** wavevector refined to a value close to the rational fraction 9/16 = 0.5625 (within one unit of standard uncertainty), the structure could not be considered *a priori* as incommensurately modulated. The data collection details are gathered in Table 1.

2.3. Data processing

All data treatment was carried out with the *JANA*98 program package (Petricek & Dusek, 1998). The measured intensities were corrected for decay (CAD-4 set only) and Lorentz–polarization effects (CAD-4 and IPDS sets). Prior to the Gaussian analytical absorption correction, the crystal shape and dimensions were optimized on the basis of equivalent reflections by means of the Stoe (1996) *X-Shape* program. Both data sets were then scaled to the same level from common reflections with $I > 10\sigma(I)$. Those reflections were then merged according to the $(\bar{3}m,\bar{1}1)$ (3 + 1)D point group, with $R_{int}(I) = 0.058$ for the observed reflections [$I \geq 2\sigma(I)$]. The original set of 28 135 reflections yielded 1084 observed independent reflections for refinement. See Table 1 for complementary information.

2.4. Structure determination and refinement

Although a 3D-space refinement approach could be attempted, given the high symmetry and the not too large period of the superstructure, a higher-dimension space method was preferred. Indeed, the use of higher-dimension crystallography has several advantages over the 3D approach: (i) it allows a unique description of the various existing phases, whatever the stoichiometry; (ii) it provides a model which can easily be compared to the oxide counterparts; (iii) it allows, in some cases, usually when satellite reflections are very weak and cannot be observed up to high orders, a possible reduction of the number of refined parameters (in a 3D approach this would lead to parameter correlation). The easiest way to carry out (3 + 1)D structure refinement is to consider, initially, that the structure is incommensurate. Then, given the apparent commensurateness of the wavevector **q**, a commensurate test can be performed.

The observed reflection extinction rules (*hklm*: $h - k - l = 3n$; *hhlm*: $m = 2n$) suggested $R\bar{3}m(00\gamma)0s$ as a possible superspace group, as in the oxide series. Consequently, the structure refinement was initiated with the model developed for the hexagonal perovskite oxides (Evain *et al.*, 1998;

Gourdon *et al.*, 1999). In brief, this model involves the introduction of occupation crenel functions for the description of both the O atoms and the metal atoms, which nicely determines the succession of face-sharing octahedra and trigonal prisms in the $[MO_3]$ chain subsystem and allows a good modelling of the metal coordination (see below). However, it rapidly became apparent that the model adopted for the oxide series could not be applied to the $Sr_{9/8}TiS_3$ sulfide structure. Indeed, although a large number of displacive waves were introduced for all atoms, very large residues (up to 15 e Å^{-3}) were observed in the difference Fourier maps and non-physical distances were calculated. A strategy similar to that adopted for $Sr_{1.2872}NiO_3$ (Evain *et al.*, 1998) was then devised.

In a first step, the structural model proposed by Ukei *et al.* (1993) for $[Ba]_x(Pt,Cu)O_3$ and Onoda *et al.* (1993) for $Sr_{1.145}TiS_3$ was used as a starting point for the refinement. The structure is described in the $R3m(00\gamma)0s$ non-centrosymmetric superspace group, which gives full occupancy for the two independent atoms of the $[TiS_3]$ first subsystem [Ti at $(0,0,w)$, $w \simeq 0$; S at $(2u,u,w)$, $u \simeq 0.08$ and $w \simeq 0.5$] and full occupancy for the only independent atom of the [Sr] second subsystem [Sr at (1/3,0,1/4)]. Note that Sr was placed at $z = 1/4$ and not at $z = 0$ as in Ukei's original structure, in order to be compatible with the centrosymmetric option of the subsequent refinements (see below). Starting from the average structure, the positions and Debye–Waller factors (DWF) of the three independent atoms were modulated up to rather high orders (sixth order for the positions and fourth order for the DWFs), although yielding a poor fit with $R = 11.1\%$ for 95 parameters and 1035 independents reflections at a 2σ cutoff (note that all refinements were carried out on F^2 with all reflections included, but that the reported residual values are for observed reflections only). During the course of the structure determination of $Sr_{1.2872}NiO_3$ (Evain *et al.*, 1998), it was observed that the O atom placed on the $(m_x 1|0,0,0,1/2)$ symmetry element (labelled O) was always shifted through the displacive modulations either towards the *A* position or towards the *B* position (see Figs. 1*a* and 2*a*) and the atom was therefore split into two parts (*A* and *B*, respectively) *via* crenel functions, using the $R\bar{3}m(00\gamma)0s$ centrosymmetric space group (see Fig. 3*a*). The fact that the O atoms cannot occupy both *A* and *B* positions at the same *z* elevation and that there is always one position at a given *z* coordinate, set the crenel widths and centres (Δ and $\hat{x}_4$, respectively; see Fig. 3*a*). In $Sr_{9/8}TiS_3$, the situation is far more complicated, with the S-atom line divided into six disjointed rods along one period of the internal coordinate in the (3 + 1)D space (see Figs. 1*b* and 2*b*). However, out of the six fragments only two are symmetry independent, which will be labelled S1 and S2.

To define the S1 rods, an S atom was introduced on the $(2_{xy}\,\bar{1}|0,0,0,1/2)$ axis at $(x,x,1/2)$, $x \simeq 0.17$, with its occupancy limited by a crenel function, centred at $\hat{x}_4^{S1(A)} = 1/4$ (as implied by symmetry) and of width $\Delta^{S1(A)} \simeq 0.375$. The latter value was initially determined from F_{obs} synthesis maps and refined (incommensurate approach), and later deduced from the γ component of the wavevector **q**, in agreement with the polyhedron succession, and fixed accordingly to 0.375 (commensurate approach, see below). In a similar way, the S2 rods were taken into account by an S position introduced on the

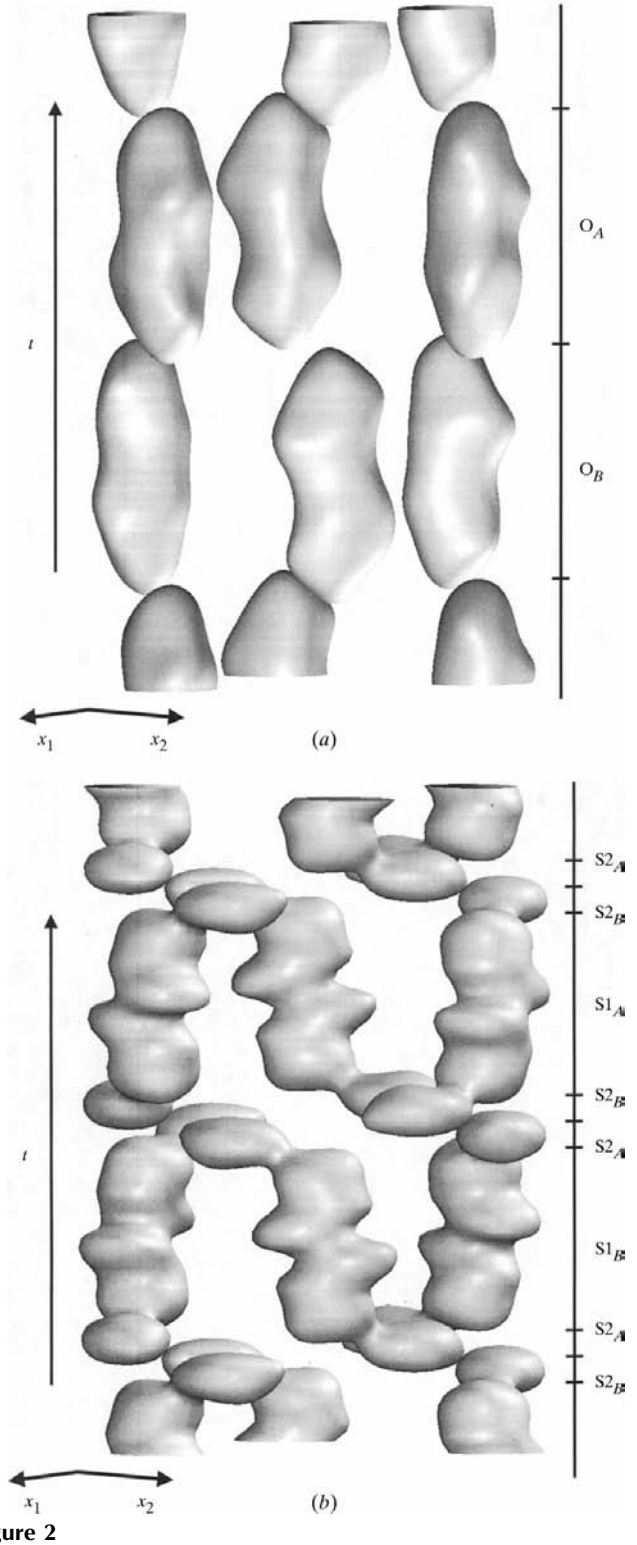

Figure 2
Tridimensional x_1x_2 *versus* the internal coordinate *t* F_{calc} synthesis isosurfaces illustrating (*a*) the oxygen modulation in $Sr_{1.2872}NiO_3$ (Evain *et al.*, 1998; isovalue 10 e Å^{-3}) and (*b*) the sulfur modulation in $Sr_{9/8}TiS_3$ (isovalue 10 e Å^{-3}). Note that F_{obs} synthesis isosurfaces (not shown) provide the same information, but with additional noise. The two figures are to be related to the projections presented in Figs. 1(*a*) and (*b*), respectively.

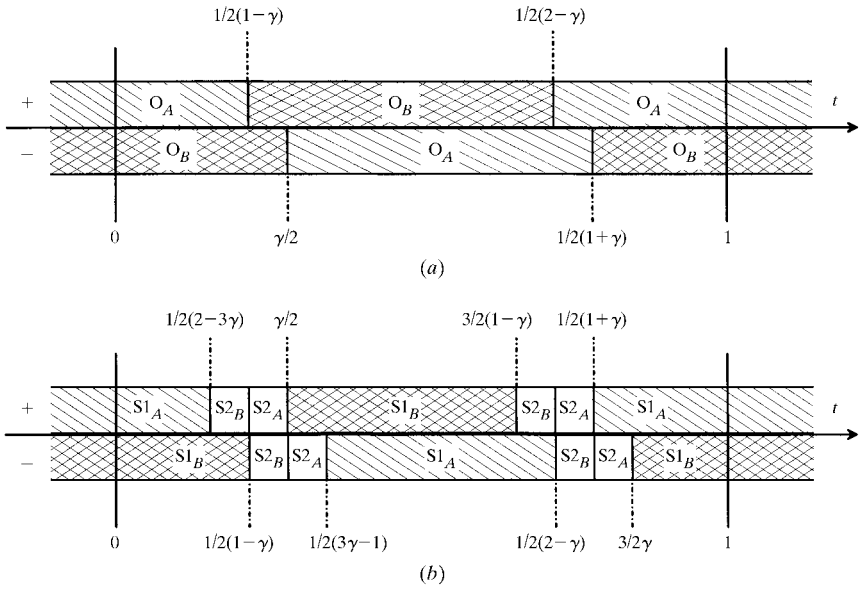

Figure 3
Domain limits, as a function of the internal t coordinate, of the crenels used in the $Sr_{9/8}TiS_3$ structure determination, using (*a*) the model developed for $Sr_{1.2872}NiO_3$ (Evain *et al.*, 1998) and (*b*) the new proposed model. Note that, for convenience, the S2 z coordinate is assumed to be exactly 1/2 in (*b*).

$(m_x\,1|0,0,0,1/2)$ mirror at $(x,2x,z)$, $x \simeq 0.095$ and $z \simeq 0.5$, with its occupancy defined by a crenel function constrained to the S1 crenel by

$$\Delta^{S2(A)} = 1/4 - 1/2\Delta^{S1(A)}$$

and

$$\hat{x}_4^{S2(A)} = 1/2[\hat{x}_4^{S1(A)} - 1/2\Delta^{S1(A)}].$$

Such a splitting of the original S position is presented in Fig. 3(*b*) as a function of t, instead of x_4, for the set of positions at $z \simeq 1/2$ (top part with the + sign) and the set of positions at $z \simeq -1/2$ (bottom part with the − sign). One should remember that both sets of positions do not correspond because of the $t = x_4 - \mathbf{q}\cdot\mathbf{r}$ dependence. The related x_3 *versus* x_4 representation is presented in Fig. 4(*b*) and its oxide counterpart in Fig. 4(*a*). With this model, refining one crenel width parameter and reducing the number of waves for the S atoms (third order for position and DWF of S1 and none for S2),

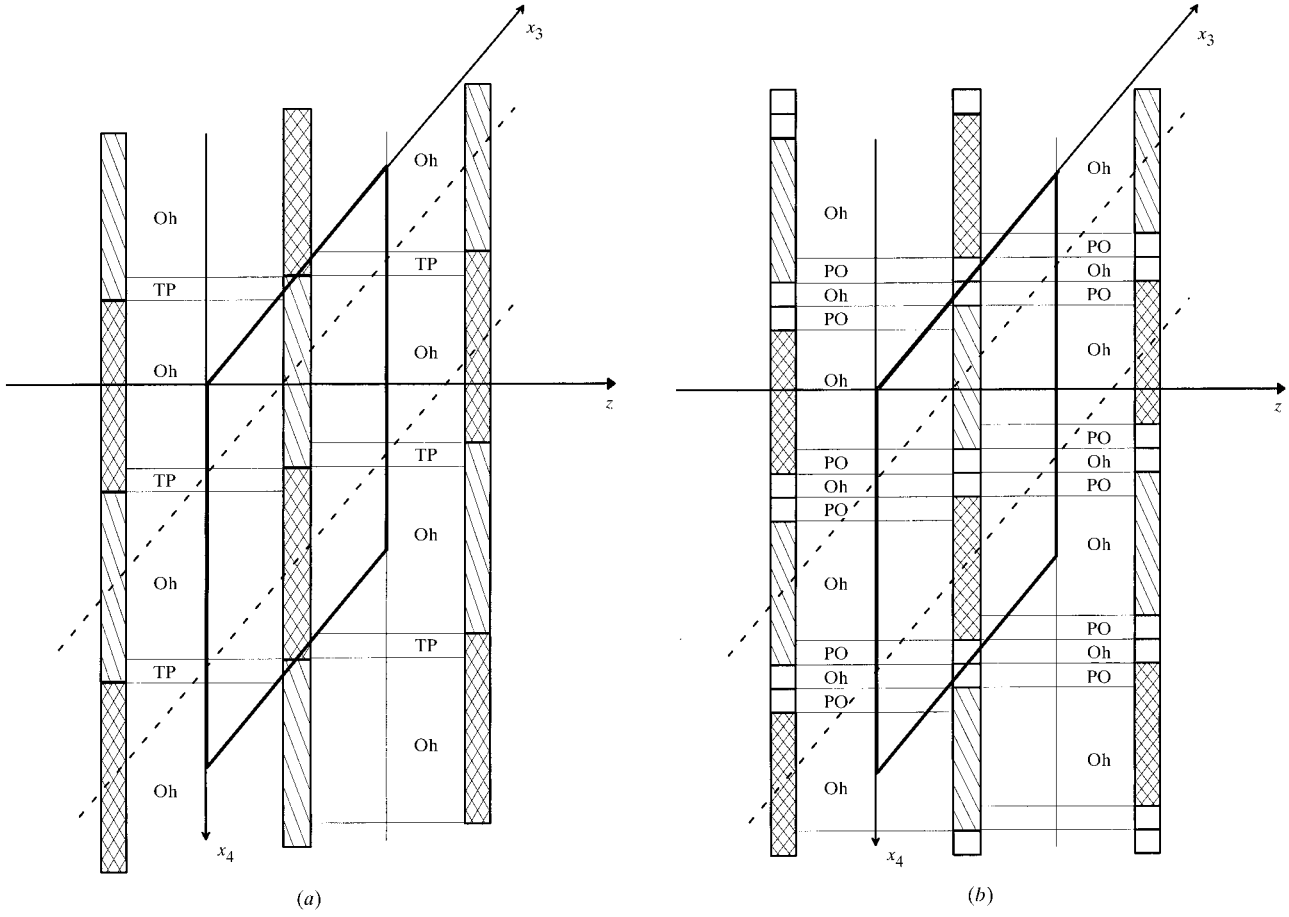

Figure 4
Superspace x_3x_4 section for $Sr_{9/8}TiS_3$ using (*a*) the model developed for $Sr_{1.2872}NiO_3$ (Evain *et al.*, 1998) and (*b*) the new proposed model. The crenels used for sulfur atoms (located at $x_3 = 1/2$) are highlighted by various hatching patterns and the resulting metal environments (metal atoms at $x_3 = 0$) are indicated by labels (Oh, TP and PO). The strontium positions are indicated by the dashed lines.

the residual factor for observed reflections [$2\sigma(I)$ level] became established at 7.8%. Note that the set of harmonic functions were orthogonalized for a smooth refinement convergence (Petricek *et al.*, 1995). Indeed, the application of crenel functions without orthogonalization would lead to modulation functions that were not defined for all $\hat{x}_4$ values and therefore prone to severe correlation.

Addition of displacement and DWF harmonics of Sr (up to the tenth order for displacement and to the sixth order for DWF) did not improve the fit (R = 7.4% with 72 parameters), although the major residues observed in the difference Fourier maps were located around the Sr position. Given the apparent commensurateness of the **q** vector components, a procedure taking into account possible reflection overlap was attempted.

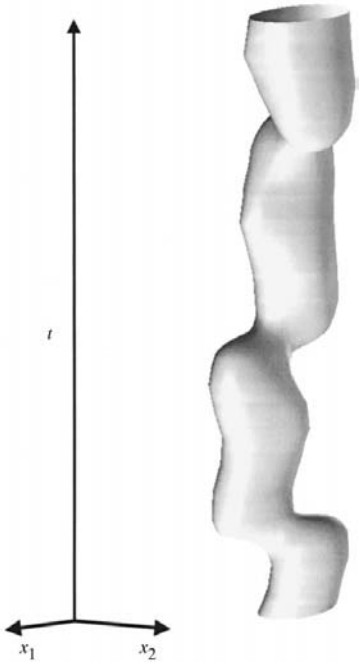

Figure 5
Tridimensional x_1x_2 *versus* the internal t coordinate F_{calc} synthesis isosurfaces illustrating the strontium modulation in $Sr_{9/8}TiS_3$ (isovalue 50 e Å^{-3}).

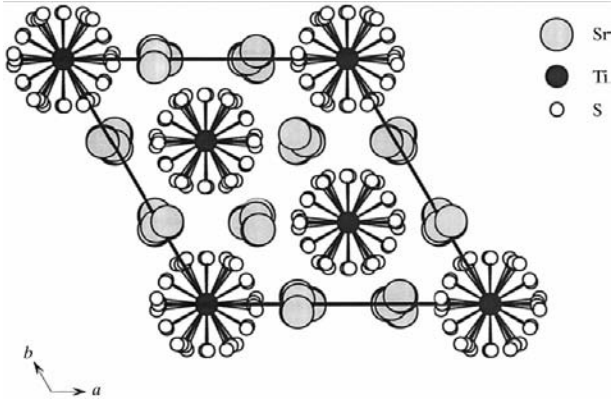

Figure 6
Projection along c of the $Sr_{9/8}TiS_3$ structure from which the two [TiS_3] and Sr chain subsystems can be easily identified.

This option consisted of combining each (h,k,l,m) reflection intensity with the (h,k,l,m) $\pm$ (0,0,9,−16) neighbouring reflection intensities. A substantial drop of the residual factor was then observed (R = 6.2%), with an important effect on the highest-order satellites. At this stage, an analysis of the atomic modulation of Sr (x displacement for instance; see Fig. 5) suggested crenel-like behaviour with three distinct t segments. Introduction of a crenel function for Sr (of width 1/3 and centred at the origin), orthogonalized to facilitate refinement, and reduction of harmonics (first order only for both Sr displacement and DWF) dramatically improved the refinement, with R reducing to 3.93%, for only 61 parameters. Addition of waves for Sr (third order for both displacement and DWF) slightly enhanced the results, with R = 3.61%, but with many additional parameters (79 parameters in total).

Given the improvement obtained with the overlap option (see above), a test of commensurateness was then carried out. The possible 3D space groups that correspond to a given t section have been derived already for the $R\bar{3}m(00\gamma)0s$ superspace group (Evain *et al.*, 1998). With the γ component of the wavevector **q** close to the 9/16 rational ratio, only two R-centred space groups are possible: $R\bar{3}c$ and $R3c$. Starting with the highest symmetry, $R\bar{3}c$ obtained for instance with t = 0, and fixing the S crenel widths according to the values obtained in the incommensurate refinement [$\Delta^{S1(A)}$ = 0.3747 (9)], the

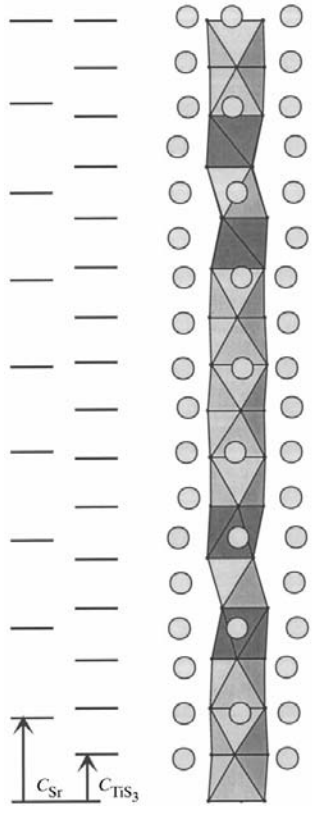

Figure 7
Development along the c axis (arbitrary orientation) of the [TiS_3] chain and its neighbouring Sr atoms for the $Sr_{9/8}TiS_3$ structure [(3 + 1)D commensurate model] showing the succession of PO and Oh TiS_6 entities. The periodicities of both subsystems are also indicated.

Table 2
Final residual factors for $Sr_{1.125}TiS_3$ [commensurate (3 + 1)D option].

	Number	*R*	*wR*
Main	250	2.70	4.52
First order	278	2.23	4.30
Second order	193	2.94	5.45
Third order	180	3.86	6.87
Fourth order	183	3.25	5.41
Overall	1084	2.79	4.94
TiS_3 part	91	2.57	4.66
Sr part	133	3.07	4.49
Common	26	1.79	4.21

refinement swiftly converged with a significant drop of the residual *R* to the value of 2.88% for only 60 parameters. Changing the S1 crenel width to the 6 × 1/16 = 0.375 commensurate value had no influence on the results. Note that the Sr displacement and DWF modulation waves had to be reduced to the first order, to comply with the degree of freedom allowed by the 3D symmetry. Expanding the Ti and S modulation waves to the maximum allowed order (Ti: sixth order and eighth order for position and DWF, respectively; S1: third order for position and DWF), the residual *R* value converged to the final value *R* = 2.79% [$wR(F^2)$ = 4.94%] for 64 parameters (that is, the same number as in the 3D approach) and 1084 observed reflections [*R* = 7.16% and $wR(F^2)$ = 5.85% for the whole set of 1643 reflections]. A test of the second possible 3D space-group choice (*R*3*c*) did not yield better results. Note that to achieve an equivalent *R* value with the incommensurate approach, we had to add about 30 parameters and take into account satellite-reflection overlap. Therefore, we considered the commensurate approach as the best refinement, although the commensurate/incommensurate discrimination is not really important for such a long-period misfit compound. Final parameters for the commensurate (3 + 1)D model are gathered in Tables 2, 3 and 4.[1]

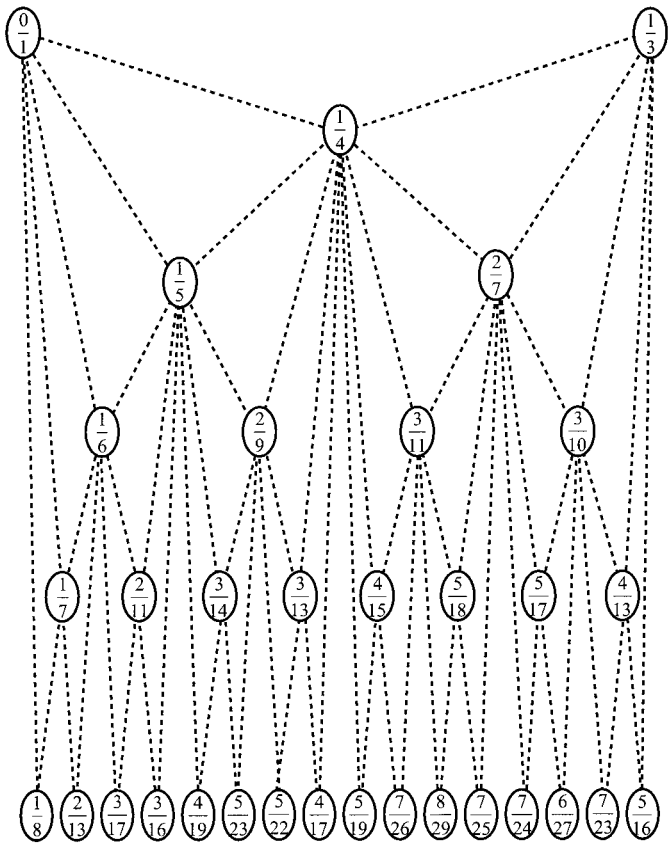

Figure 8
Farey tree (*Royal Society Mathematical Tables*, 1950) within the [0,1/3] *x* interval.

Table 3
Fractional atomic coordinates and equivalent isotropic displacement parameters (Å^2) for $Sr_{1.125}TiS_3$ [commensurate (3 + 1)D option].

$B_{eq} = (8\pi^2/3)\sum_i\sum_j U^{ij}a_i^*a_j^*\mathbf{a}_i\mathbf{a}_j$.

	x	*y*	*z*	B_{eq}
Sr	0.35983 (3)	0	1/4	1.494 (10)
Ti	0	0	0	1.029 (13)
S1	0.16935 (5)	0.16935	1/2	1.06 (2)
S2	0.0979 (2)	0.18794 (12)	0.5183 (4)	2.21 (4)

3. Discussion

The crystal structure of $Sr_{9/8}TiS_3$ is quite different from that reported by Onoda *et al.* (1993) for the, *a priori*, analogous compound $Sr_{1.145}TiS_3$. Indeed $Sr_{1.145}TiS_3$ was described (Onoda *et al.*, 1993) with a structural model resembling those used for the hexagonal perovskite-type oxides. That is, the structure was determined as built from two infinite chains, [Sr] and [TiS_3], the latter being a succession of [TiS_6] face-sharing octahedra and trigonal prisms. The $Sr_{9/8}TiS_3$ structure reported herein is also built from [Sr] and [TiS_3] infinite chains (see Fig. 6), but there are no trigonal prisms among the [TiS_6] units. The difference between the oxide structures and the $Sr_{9/8}TiS_3$ structure was perceived during the structure refinement since the oxide structural model developed for $Sr_{1.2872}NiO_3$ (Evain *et al.*, 1998) and $Sr_{14/11}CoO_3$ (Gourdon *et al.*, 1999) could not be used for $Sr_{9/8}TiS_3$, a new description of the chalcogen atom being devised through the establishment of a more complex crenel system (see above). A new [TiS_6] polyhedron appears, intermediate between a trigonal prism (TP) and an octahedron (Oh), which we will hereinafter label as PO. It is worth noting that these new PO sites always occur in pairs surrounding an octahedron (*i.e.* in PO–Oh–PO groups) in the [TiS_3] chain. The hexagonal perovskite-type sulfides can therefore be described as the hexagonal perovskite-type oxides, after replacing the oxide TP sites by sulfide PO–Oh–PO entities.

[1] Supplementary data for this paper, including atomic positional and DWF modulation coefficients [(3 + 1)D option], orthonormalized set functions used for modulation [(3 + 1)D option], fractional atomic coordinates and equivalent isotropic displacement parameters (3D option), and *hkl* values, are available from the IUCr electronic archives (Reference: LC0021). Services for accessing these data are described at the back of the journal.

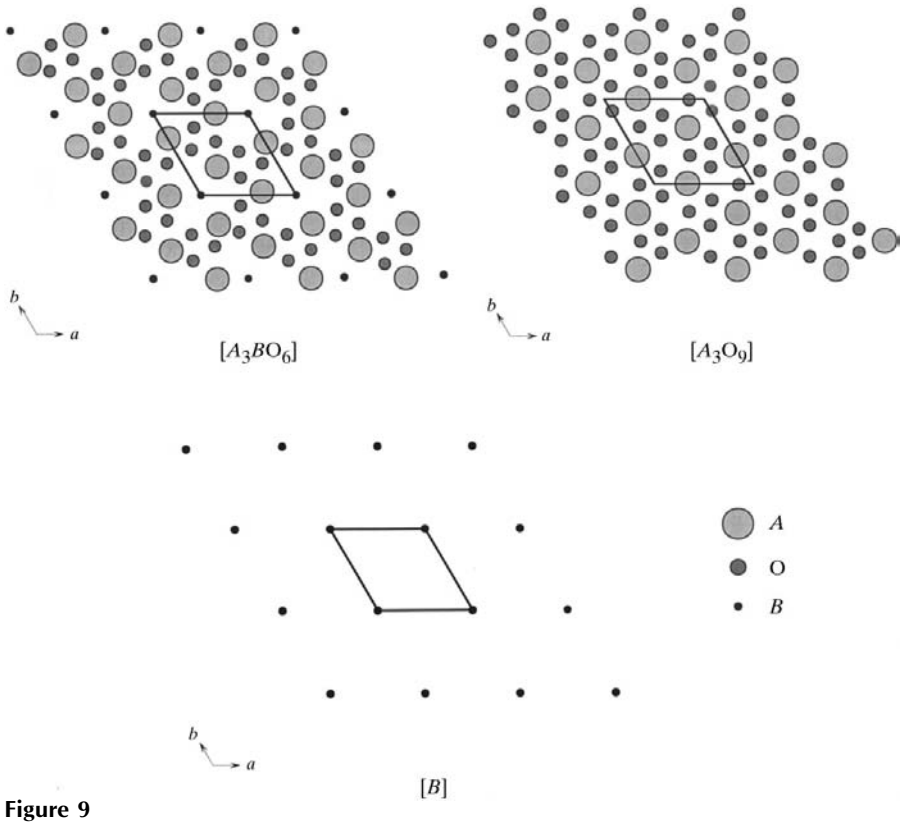

Figure 9
Schematic view of the different planes which can be used to build up a hexagonal perovskite-like oxide structure. For example, $Ba_6Ni_5O_{15}$ can be considered as the succession of the $-[Ba_3O_9]-[Ni]_2-[Ba_3NiO_6]-[Ni]_2-$ layers.

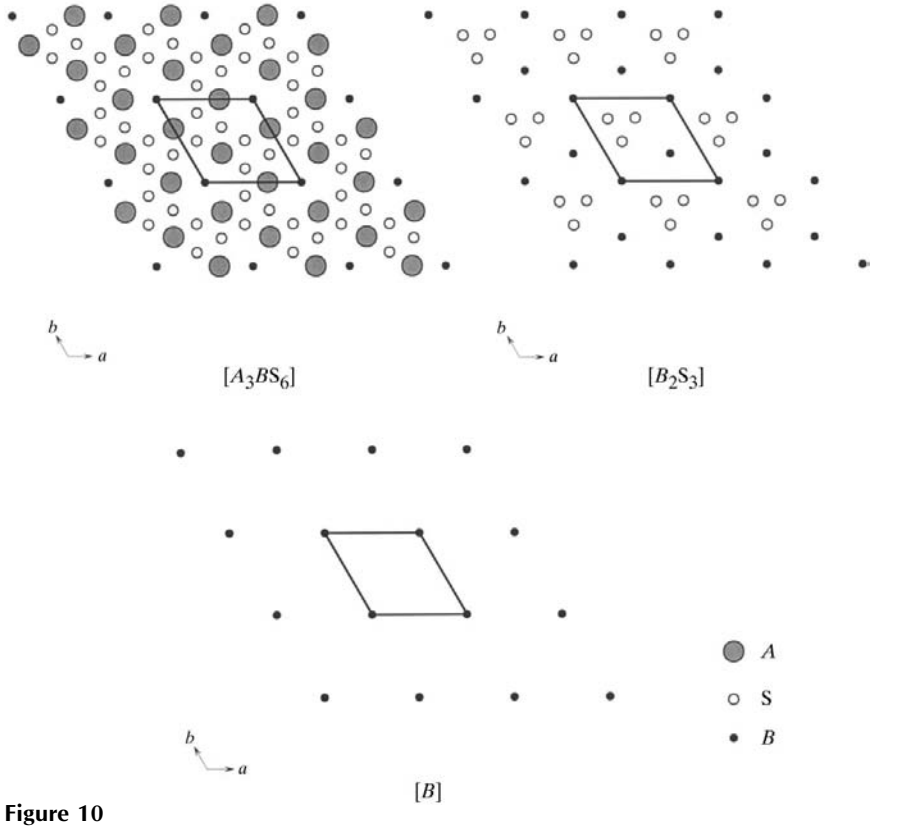

Figure 10
Schematic view of the different planes which can be used to build up the $Sr_{9/8}TiS_3$ hexagonal perovskite-like sulfide structure. The observed sequence is as follows: $-[Sr_3TiS_6]-[Ti]-[Sr_3TiS_6]-[Ti_2S_3]-[Sr_3TiS_6]-[Ti_2S_3]-$.

The periodic polyhedron succession in the $Sr_{9/8}TiS_3$ $[TiS_3]$ chains is $[-(Oh)_5-(PO-Oh-PO)-(Oh)_5-(PO-Oh-PO)-]$, as shown in Figs. 4(*b*) and 7. For the hexagonal perovskite-type oxide, it has been shown (Evain *et al.*, 1998) that the succession of the Oh and TP polyhedra could be deduced from the γ component of the wavevector **q**, or equivalently from the composition since it can be expressed as $A_{2\gamma}BX_3$, with $\gamma = m/n$ for the commensurate cases. Perez-Mato *et al.* (1999) then proposed a convenient way of giving the succession of Oh and TP prisms from the composition value $x = 2\gamma - 1$ by using the Farey tree (Royal Society Mathematical Tables, 1950) within the [0,1/2] x interval. Although there are few fully resolved hexagonal perovskite-type sulfides (Gourdon *et al.*, 2000), it seems that the Oh and PO sequence in an $A_{1+x}BS_3$ compound can also be given by a Farey tree limited to the [0,1/3] interval (Fig. 8). The determination of the sequence is as follows: after locating in the tree the $x = i/j$ fraction (i and j are integers), the prism succession in the $[BS_3]$ chains is obtained by juxtaposition of the sequences corresponding to the two fractions i_1/j_1 and i_2/j_2 used to build the tree branch (with $i = i_1 + i_2$ and $j = j_1 + j_2$). The starting fractions correspond to one Oh for $x = 0/1$ and one PO–Oh–PO unit for $x = 1/3$. For $\gamma = 9/16$, $x = 1/8$ and thus the sequence is $-(Oh)_5-(PO-Oh-PO)-$. $x = 1/3$ would correspond to the $-(PO-Oh-PO)-(PO-Oh-PO)-$ prism succession, which is not certain to occur in real compounds since it involves the juxtaposition of two PO units (the analogue juxtaposition of two TP has been ruled out in oxides since it has never been found).

It has been shown (Darriet & Subramanian, 1995) that an $A_{1+x}BO_3$ hexagonal perovskite-type oxide structure can be considered as a stacking of $[A_3O_9]$ and $[A_3BO_6]$ layers sandwiching B-metal layers. The $[A_3O_9]$ layer derives from the $[A_3BO_6]$ layer by substituting one B atom for three O atoms (see Fig. 9). The composition limits, ABO_3 and $A_{1.5}BO_3$, are obtained for $[A_3O_9]$ layers only and for a succession of $[A_3O_9]$ and $[A_3BO_6]$ layers, respectively. Note that the layers are usually not well defined

Table 4
Anisotropic displacement parameters U^{ij} (Å^2) for $Sr_{1.125}TiS_3$ [commensurate (3 + 1)D option].

The anisotropic displacement factor exponent takes the form $-2\pi^2 \sum_i \sum_j U^{ij} a_i^* a_j^* \mathbf{h}_i \mathbf{h}_j$.

	U^{11}	U^{22}	U^{33}	U^{12}	U^{13}	U^{23}
Sr	0.01631 (14)	0.0201 (2)	0.0216 (2)	0.01004 (9)	−0.00406 (7)	−0.0081 (2)
Ti	0.0138 (2)	0.0138	0.0116 (3)	0.00688 (9)	0	0
S1	0.0124 (2)	0.0124	0.0102 (3)	0.0022 (2)	−0.00013 (12)	0.00013
S2	0.0421 (8)	0.0122 (5)	0.0202 (6)	0.0066 (5)	0.0143 (6)	0.0003 (5)

(*i.e.* flat), because the height of the [BO_6] trigonal prism is generally far from twice the height of the [BO_6] octahedron. The $Sr_{9/8}TiS_3$ structure can also be described as a stacking of layers. However, the layers are different. In fact, the $Sr_{9/8}TiS_3$ structure can be described as [Sr_3TiS_6] layers that alternate with either [Ti] or [Ti_2S_3] layers (see Fig. 10). The Ti atoms of the [Ti] or [Ti_2S_3] layers are always in Oh sites. When a [Sr_3TiS_6] layer is surrounded by two [Ti_2S_3] layers, its Ti metals are also in Oh sites, but when it is surrounded on one side by a [Ti] layer and on the other side by a [Ti_2S_3] layer, it leads to the original PO coordination (see Fig. 11). It is worth noting that the PO and Oh sites are very similar in height, which gives rather well defined layers.

In Table 5, the main Sr–S distances are presented. A thorough analysis of these distances shows that the shortest distances are found when the Sr atoms are facing a [TiS_3] chain at the metal elevation [PO and Oh sites of the –(PO–Oh–PO)– groups only], and the longest distances when the Sr atoms are facing a [TiS_3] chain at the S elevation. Since each Sr atom is surrounded by three [TiS_3] chains, two at the S elevation and one at the metal elevation (see Fig. 10*a*), to avoid shorter distances, Sr is displaced within the *xy* plane, away from the metal. This displacement could not be included in the refinement *via* modulations and was taken into account through the introduction of a crenel function for the Sr atoms (see above). This is readily visualized in Fig. 6, yielding three groups of Sr atoms for each [Sr] chain.

The Ti–S distances are rather uniform, ranging from 2.41 to 2.47 Å whatever the coordination, as shown in Fig. 12(*a*). This is quite different from the situation found in the oxide where two sets of distances were observed, with long and short distances associated with the TP site and +II oxidation state, and the Oh site and +IV oxidation state, respectively. In addition, in $Sr_{9/8}TiS_3$, the Ti–Ti distances (Fig. 12*b*) fluctuate in a large domain, from 2.79 to 3.14 Å. Both observations suggest a more subtle charge balance for the sulfides than for the oxides. One can easily show (from the crenel width in Fig. 3 for instance) that the ratio of Oh to PO sites is equal to $(3n - 4m)/(4m - 2n)$, with $\gamma = m/n$ (in an equivalent way, one can obtain this ratio from $x = i/j$ using the Farey tree). A general formula

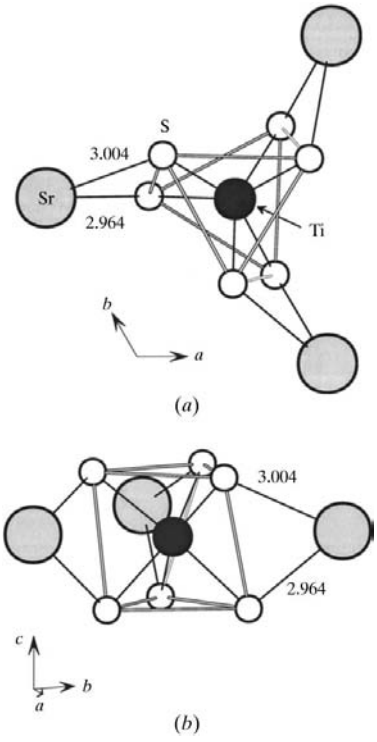

Figure 11
Ti environment and Sr—S distances (Å) in a PO site.

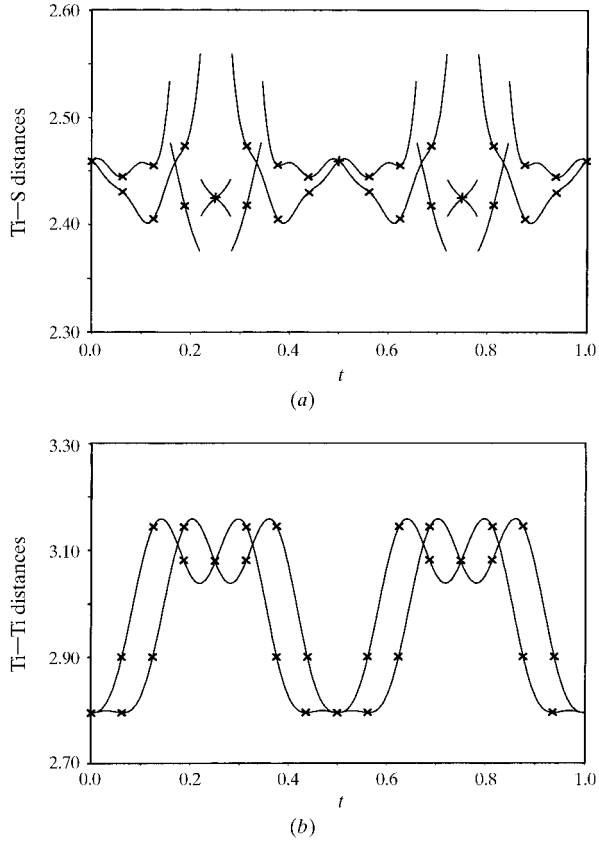

Figure 12
(*a*) Ti—S and (*b*) Ti—Ti distances (Å) as a function of the internal *t* coordinate for the $Sr_{9/8}TiS_3$ (3 + 1)D commensurate model. The crosses correspond to the equivalent distances calculated from the 3D commensurate approximation.

Table 5
Main Sr—S distances (Å).

Shortest Sr—S distances		Longest Sr—S distances	
Sr—S2	2.9778 (11) (2×)	Sr—S1	3.1076 (13)
Sr—S2	3.0056 (13)	Sr—S1	3.1152 (10) (2×)
Sr—S1	2.9627 (12)	Sr—S1	3.1298 (12)
Sr—S1	2.9937 (10)	Sr—S1	3.158 (2) (2×)
		Sr—S1	3.1664 (12)
		Sr—S1	3.265 (2)
		Sr—S1	3.268 (2)
		Sr—S1	3.340 (2) (2×)

can then be proposed for the hexagonal perovskite-like sulfides: $A_{2m}B'_{4m-2n}B_{3n-4m}S_{3n}$, with B' and B in PO and Oh sites, respectively. An obvious formal charge assignment corresponds B'^{III} and B^{IV}, as clearly seen from the rearranged formula: $(A_3B'_2S_6)_{2m-n}(ABS_3)_{3n-4m}$ or, equivalently, $(A_3B'_2S_6)_{2\gamma-1}(ABS_3)_{3-4\gamma}$ or $(A_3B'_2S_6)_x(ABS_3)_{1-2x}$. However, our preliminary *ab initio* band-structure calculations suggest that the highest oxidation state would correspond to the metal in PO sites, *i.e.* in contradiction with the straightforward charge balance.

4. Conclusions

A new hexagonal perovskite-like sulfide compound, $Sr_{9/8}TiS_3$, was obtained and its structure solved using higher-dimension crystallography. Unlike the oxide counterparts, the $[TiS_3]$ chains of $Sr_{9/8}TiS_3$ are built from face-sharing octahedra and distorted PO prisms, intermediate between octahedra and trigonal prisms, and not simply from face-sharing octahedra and trigonal prisms. This new pattern seems to be common to all hexagonal perovskite-like sulfides, as demonstrated by other partly solved structures, such as that of $Sr_{8/7}TiS_3$, $Eu_{8/7}TiS_3$ or $Sr_{1.1054}TiS_3$ (Gourdon *et al.*, 2000). This disagrees with the previously reported structure for $Sr_{1.145}TiS_3$ (Onoda *et al.*, 1993), which suggested trigonal prisms and octahedra as coordination spheres for the Ti metal atoms. It is, however, in agreement with the usual stability of Ti in an S environment. A simple charge assignment leads to Ti^{III} and Ti^{IV} in PO and Oh sites, respectively. However, this is not in agreement with our preliminary *ab initio* band-structure calculations. Extended band-structure calculations and physical measurements are currently in progress to help analyse and understand the electron density distribution in such compounds and, more generally, their overall stability.

References

Darriet, J. & Subramanian, M. A. (1995). *J. Mater. Chem.* **5**, 543–552.
Dussarat, C., Grasset, F. & Darriet, J. (1995). *Eur. J. Solid State Inorg. Chem.* **32**, 557–576.
Evain, M. (1992). *U-Fit. A Cell Parameter Refinement Program.* Nantes: Institut des Matériaux.
Evain, M., Boucher, F., Gourdon, O., Petricek, V., Dusek, M. & Bezdicka, P. (1998). *Chem. Mater.* **10**, 3068–3076.
Gourdon, O., Petricek, V., Dusek, M., Bezdicka, P., Durovic, S., Gyepesova, D. & Evain, M. (1999). *Acta Cryst.* B**55**, 841–848.
Gourdon, O., Petricek, V. & Evain, M. (2000). *Z. Kristallogr.* Submitted.
Janssen, T., Janner, A., Looijenga-Vos, A. & de Wolff, P. M. (1993). *International Tables for X-ray Crystallography*, Vol. C, *Mathematical, Physical and Chemical Tables*, edited by A. J. C. Wilson, ch. 9.8. Dordrecht: Kluwer Academic Publishers.
Onoda, M., Saeki, M., Yamamoto, A. & Kato, K. (1993). *Acta Cryst.* B**49**, 929–936.
Perez-Mato, J. M., Zakhour-Nakhl, M., Weill, F. & Darriet, J. (1999). *J. Mater. Chem.* **9**, 2795–2808.
Petricek, V. & Dusek, M. (1998). *JANA*98. *Programs for Modulated and Composite Crystals*. Institute of Physics, Praha, Czech Republic.
Petricek, V., van de Lee, A. & Evain, M. (1995). *Acta Cryst.* A**51**, 529–535.
Royal Society Mathematical Tables (1950). Vol. I. *The Farey Series of Order 1025*. Royal Society/Cambridge University Press.
Saeki, M. & Onoda, M. (1993). *J. Solid State Chem.* **102**, 100–105.
Saeki, M. & Onoda, M. (1994). *J. Solid State Chem.* **112**, 65–69.
Saeki, M., Onoda, M. & Yajima, Y. (1996). *J. Solid State Chem.* **121**, 451–456.
Smaalen, S. van (1995). *Crystallogr. Rev.* **4**, 79–20.
Stoe (1996). *X-Shape*. *Crystal Optimization for Numerical Absorption Correction*. Stoe & Cie Gmbh, Darmstadt, Germany.
Ukei, K., Yamamoto, A., Watanabe, Y., Shishido, T. & Fukuda, T. (1993). *Acta Cryst.* B**49**, 67–72.